Chapter 11

The Indian Ocean

We now turn to the Indian Ocean, which is in several respects very different from the Pacific Ocean. The most striking difference is the seasonal reversal of the monsoon winds and its effects on the ocean currents in the northern hemisphere. The absence of a temperate and polar region north of the equator is another peculiarity with far-reaching consequences for the circulation and hydrology.

None of the leading oceanographic research nations shares its coastlines with the Indian Ocean. Few research vessels entered it, fewer still spent much time in it. The Indian Ocean is the only ocean where due to lack of data the truly magnificent textbook of Sverdrup *et al.* (1942) missed a major water mass - the Australasian Mediterranean Water - completely. The situation did not change until only thirty years ago, when over 40 research vessels from 25 nations participated in the International Indian Ocean Expedition (IIOE) during 1962 - 1965. Its data were compiled and interpreted in an atlas (Wyrtki, 1971, reprinted 1988) which remains the major reference for Indian Ocean research. Nevertheless, important ideas did not exist or were not clearly expressed when the atlas was prepared, and the hydrography of the Indian Ocean still requires much study before a clear picture will emerge. Long-term current meter moorings were not deployed until two decades ago, notably during the INDEX campaign of 1976 - 1979; until then, the study of Indian Ocean dynamics was restricted to the analysis of ship drift data and did not reach below the surface layer.

Bottom topography

The Indian Ocean is the smallest of all oceans (including the Southern Ocean). It has a north-south extent of 9600 km from Antarctica to the inner Bay of Bengal and spans 7800 km in east-west direction between southern Africa and western Australia. Without its southern ocean part it covers an area of $48 \cdot 10^6$ km^2. If the southern ocean part is included, the area increases to $74.1 \cdot 10^6$ km^2. The only large shelf area is the Northwest Australian Shelf, a region of strong tidal dissipation. It is part of the large expanse of continental shelf between Australia and south-east Asia that continues as the Timor and Arafura Seas and the Gulf of Carpentaria; however, these latter regions are considered part of the Pacific Ocean. The Northwest Australian Shelf itself is insufficient in size to have much impact on the mean depth of the Indian Ocean, which with 3800 m is between that of the Pacific and Atlantic Oceans. Most basins show depths well below 5000 m; in the east, the *Wharton Basin* exceeds 6000 m depth. The *Arabian Sea* reaches depths below 3000 m over most of its area, while the depth in the *Bay of Bengal* decreases gradually from 4000 m south of Sri Lanka to 2000 m and less at 18°N.

Three mediterranean seas influence the hydrographic properties of Indian Ocean water masses. The Persian Gulf is the smallest of the three; with a mean depth of 25 m, a maximum depth of only 90 m, and a sill which rises barely above the mean depth its impact is not felt much beyond the Gulf of Oman. The Red Sea is a very deep basin with maximum depths around 2740 m and a mean depth near 490 m; its sill depth is about 110 m. The Australasian Mediterranean Sea, a series of very deep basins with depths exceeding 7400 m, communicates with the Indian Ocean through various passages between the Indonesian islands where the depth is in the range 1100 - 1500 m.

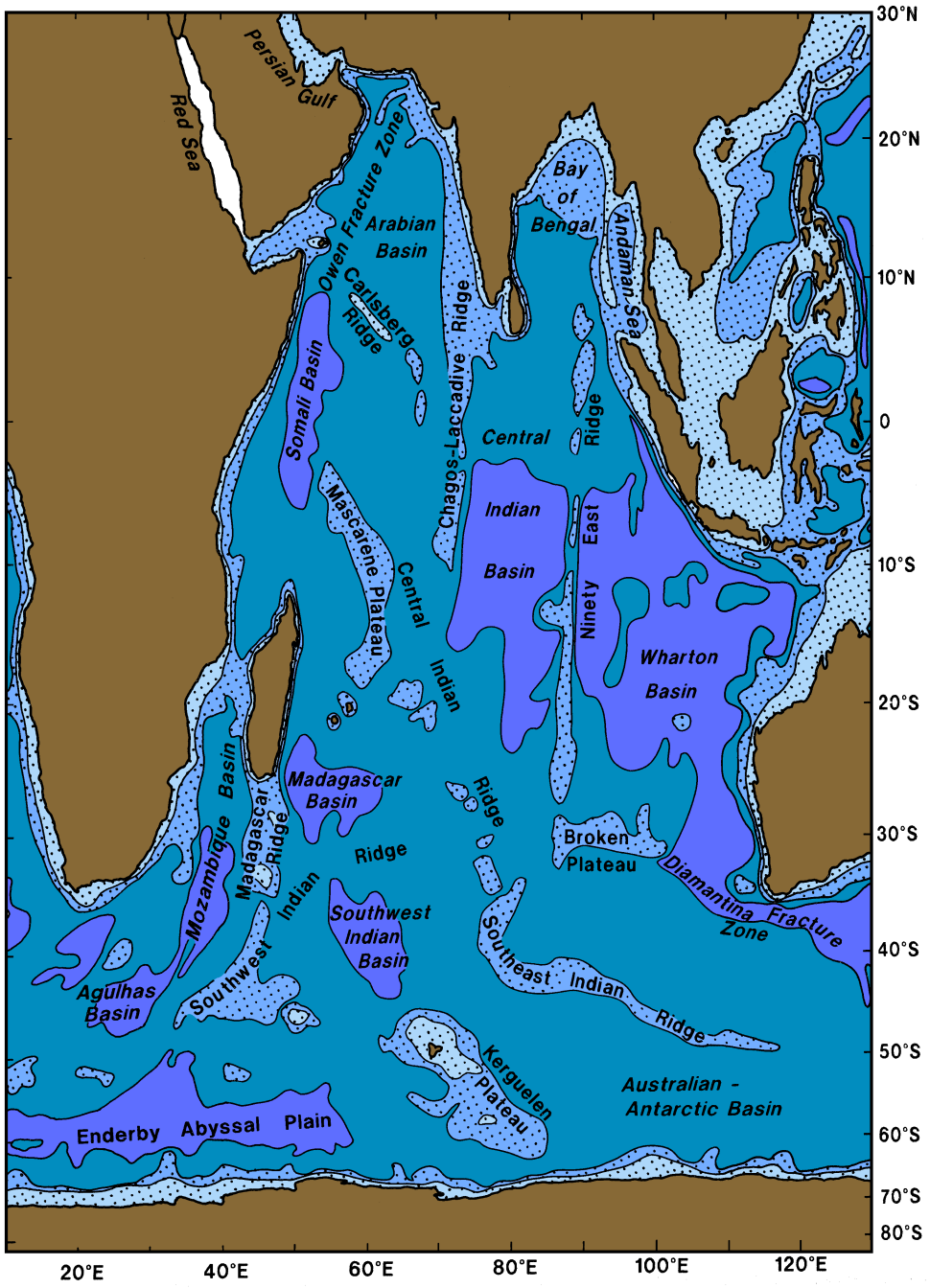

Fig. 11.1. Topography of the Indian Ocean. The 1000, 3000, and 5000 m isobaths are shown, and regions less than 3000 m deep are shaded. South of Australia the Indian Ocean extends to Tasmania (146° 55'E). See Figure 8.3 for the topography east of 125°E.

Two ridge systems run through the Indian Ocean in a roughly meridional direction, dividing it into three parts of about equal size (Figure 11.1). The *Central Indian Ridge* between the western and central part is a northward extension of the interoceanic ridge system (Figure 8.1) and connects with the ridge systems of the Atlantic and Pacific Oceans at a bifurcation point in the south. Similar to the East Pacific Rise and Mid-Atlantic Ridge it is a broad structure which rises consistently above 4000 m; again and again it reaches above 3000 m (in the region of the Mascarene Plateau it rises high enough to influence upper ocean currents), but numerous fractures and depressions make the blockage for water flow incomplete at that level. The Eastern Indian or *Ninety East Ridge* stretches in nearly perfect north-south orientation from the Andaman Islands to 33°S. It is much narrower and less fractured than the other ridges. South of 10°S it reaches the 3000 m level consistently and the 2000 m level frequently. South of 30°S it rises above 1500 m and merges with the *Southeast Indian Ridge* (a continuation of the Central Indian Ridge) at the 4000 m level. The *Broken Plateau* branches off to the east near 30°S, also reaching above 1500 m. North of 10°S the Ninety East Ridge shows occasional gaps in the 3000 m contour. The passages are apparently deeper than the merging depth of the ridge systems in the south and therefore provide a bottom water entry point for the Central Indian Basin in the northeast.

In contrast to the central and eastern parts of the Indian Ocean which are dominated by single basins of large meridional extent, the western part is subdivided by secondary ridges and the island of Madagascar into a series of smaller deep basins. The Arabian Basin is closed in the south by the merger of the *Carlsberg*, *Central Indian*, and *Chagos-Laccadive Ridges*. The merger region shows extremely complicated topography with multiple fracture zones; but the closure is complete somewhere near the 3500 m level, somewhat higher than the deepest passage in the Owen Fracture Zone. As a consequence the bottom water entry point for the Arabian Basin is also found in the north rather than in the south.

The wind regime

Monsoonal climate dominates the northern Indian Ocean, and its effects are felt far into the subtropics of the southern hemisphere. Annual mean distributions of atmospheric and oceanic parameters are therefore of only limited use. Instead, we define two mean states and discuss both separately. The information is again contained in Figs 1.2 - 1.4. A summary of the monsoon cycle is given in Figure 11.2. An introductory but comprehensive account of monsoon meteorology is given by Fein and Stephens (1987).

The *Northeast* or *Winter Monsoon* determines the climate of the northern Indian Ocean during the northern hemisphere winter (December - March). It is characterized by high pressure over the Asian land mass and northeasterly winds over the tropics and northern subtropics. The situation resembles the annual mean wind circulation over the Pacific Ocean, except that the Intertropical Convergence Zone (ITCZ) and the Doldrums are located south of the equator (near 5°S) rather than north. The wind over the northern Indian Ocean represents the Trades, but because of its seasonality it is known as the Northeast Monsoon. (The word monsoon is derived from the Arabic, meaning seasonally reversing winds.) Since most of the air pressure gradient is retained behind the Tibetan Plateau, air pressure gradients over the ocean are small. This protects the ocean from the full force of the winds blowing off the Mongolian high pressure region and results in a wind of moderate strength, comparable to the Pacific Northeast Trades which are also relatively weak at this time of

year. The wind also carries dry air, and the Winter Monsoon season is the dry season for most of southern Asia.

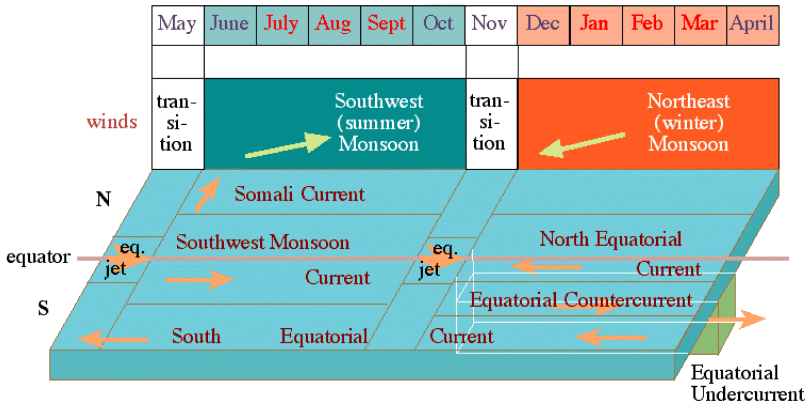

Fig. 11.2. A summary of the monsoon system in the Indian Ocean. The top part indicates the wind cycle, the lower part shows the major currents that develop in response to the wind.

The situation in the southern hemisphere is dominated by the pressure gradient between the tropical low and the subtropical high pressure belts. The axis of low pressure in the tropics is near 10°S, while the subtropical high pressure belt is dominated by an air pressure maximum 1000 km north of the Kerguelen Islands. The resulting Southeast Trades are rather uniform and somewhat stronger than in the Pacific Ocean. As in the other oceans the Trades are southerly along the eastern coast, but over Australia's Northwest Shelf winds become south-westerly, skirting the heat low over that continent. This brings summer rain to northern Australia. Rain also occurs throughout the Doldrums, with maximum rainfall in the Indonesian region.

The *Southwest* or *Summer Monsoon* determines the climate of the northern Indian Ocean during the northern hemisphere summer (June - September). A deep heat low develops over northern Arabia and Pakistan. The Australian heat low of the southern summer is replaced by a centre of high pressure, while the atmospheric high north of the Kerguelen Islands is shifted westward towards southern Africa. Whereas during the winter monsoon season the north-south pressure gradient from Arabia to Madagascar barely exceeds 6 hPa, there is now a gradient of 22 hPa acting in the opposite direction. As a result the winds in the northern Indian Ocean reverse completely and are no longer like the Trades anywhere. A wind jet, believed to be an atmospheric version of a western boundary current, develops along the high east African topography. Winds blow steadily at Beaufort 6 or more over the entire western Indian Ocean north of the equator. Further east along the equator the winds weaken, bringing moderate rainfall; but there is still a southerly component throughout the entire Indian Ocean everywhere north of 30°S. On the Northwest Shelf the wind blows directly offshore with moderate strength.

The Southwest Monsoon, as this wind is called in the northern hemisphere, is the continuation of the southern hemisphere Trades, which between 10 and 20°S are stronger, during this time of year, than anywhere else in the world. The Southwest Monsoon skirts the low over Pakistan to deposit rain on the Himalayas, thus bringing with it the monsoon rains and floods that are so crucial to Asian agriculture.

The position of the ITCZ over the ocean changes little between the seasons, but during the Southwest Monsoon frequent disturbances break away from it to settle south of the Himalayas, bringing with them most of the season's rain. Winds at the equator change direction but remain weak throughout the year. Because of their meridional orientation the associated Ekman transport does not develop a divergence at the equator. There is therefore no equatorial upwelling in the Indian Ocean. Strong equatorial downwelling occurs during the transition months (May and November) when the winds turn eastward at the equator, producing Ekman transport convergence.

Conditions for coastal upwelling are also markedly different in the Indian Ocean. Along the eastern coastline, where the most important upwelling regions of the Pacific and Atlantic Oceans are found, winds favourable for upwelling along the Australian coast are weak during the Northeast Monsoon season and absent during the Southwest Monsoon season. A small upwelling region can be expected in the latter season along the coast of Java. But the strongest upwelling of the Indian Ocean occurs along its western coastline when the Southwest Monsoon produces strong Ekman transport away from the coasts of Somalia and Arabia.

We saw in Chapter 4 that the Sverdup relation, which compares circulation patterns derived from annual mean integrated steric height and annual mean wind stress, gives very good agreement in the Indian Ocean despite the seasonal reversals of the monsoon winds. It is therefore instructive to look at the annual mean atmospheric circulation over the Indian Ocean as well. The southern hemisphere Trades stand out as particularly strong, in the annual mean, when compared with the other oceans. As we have seen, the larger contribution to this comes from the Summer Monsoon season. The stronger winds of this season dominate the annual mean in the northern Indian Ocean as well. This produces a net southwesterly stress over the northwestern Indian Ocean and in particular along the East African coast. Mean winds in the northeast and along the equator are weak and westerly.

The integrated flow

We begin the comparison between the depth-integrated flow (Figs 4.4 - 4.7) and the observed surface circulation (Figure 11.3) with the southern Indian Ocean which does not experience monsoonal winds. The Sverdrup stream function (Figure 4.7) shows a particularly strong subtropical gyre, a result of large wind stress curl between the annual mean Trades and Westerlies (Figure 1.4). South of 10°S and away from the Australian coast the pattern agrees well with the observations. Both show the South Equatorial Current being fed by the throughflow of Pacific water through the Indonesian seas and strengthening westward. The bifurcation east of Madagascar and again near the African coast is also seen in the Sverdrup flow, as is the joining of the Mozambique and East Madagascar Currents into the Agulhas Current. Furthermore, the Sverdrup relation implies net southward flow across 10°S in response to strong negative wind stress curl; this generates the eastward flowing Equatorial Countercurrent north of 10°S as its source of supply. To the best of our

knowledge, the annual mean transports of the open-ocean currents are well predicted by the Sverdrup relation, and the transports of the East Madagascar, Mozambique, and Agulhas Currents follow quite accurately from mass continuity.

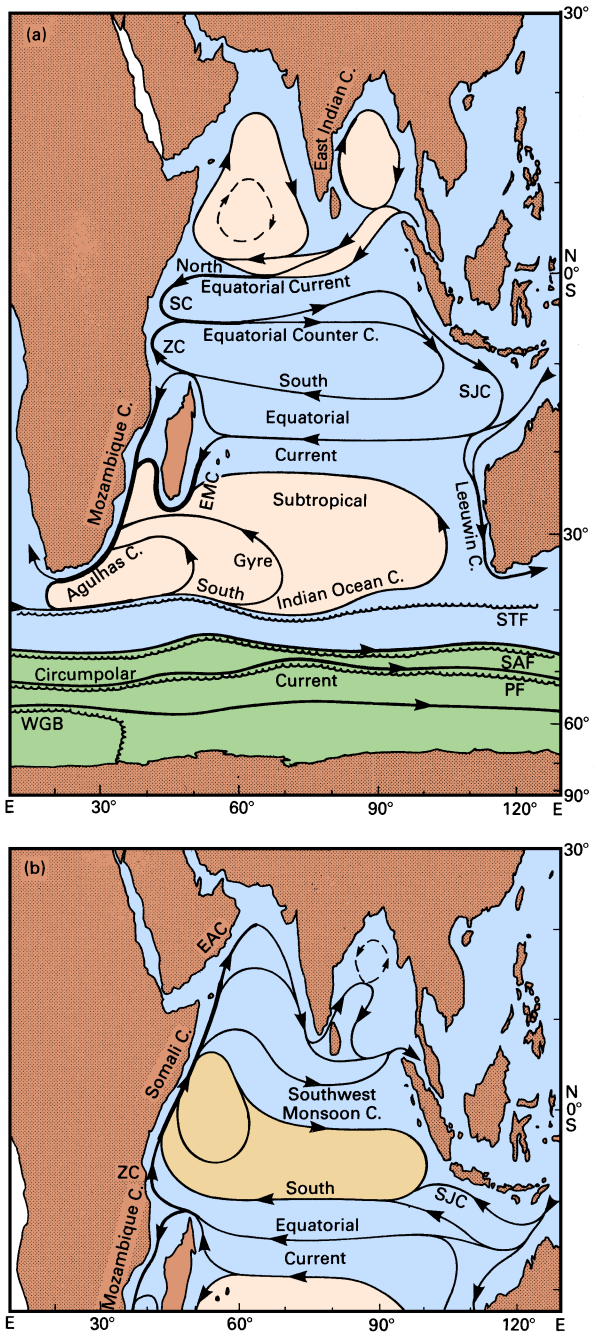

Fig. 11.3. Surface currents in the Indian Ocean.

top: late Northeast Monsoon season (March - April);

bottom: late Southwest Monsoon season (September - October; the circulation south of 20°S remains unchanged).

Abbreviations are used for the East Arabian (EAC), South Java (SJC), Zanzibar (ZC), East Madagascar (EMC), and Somali (SC) Currents. Other abbreviations denote fronts: STF: Subtropical Front, SAF: Subantarctic Front, PF: Antarctic Polar Front, WGB: Weddell Gyre Boundary.

Significant discrepancies between the Sverdrup circulation and observations are seen in the Agulhas Current extension region, for reasons discussed in Chapter 4, and in the Leeuwin Current. The net depth-averaged flow along the Australian coast is in fact very close to that given by the Sverdrup circulation; but the shallow Leeuwin Current is accompanied by an undercurrent of nearly equal transport (to be discussed below), and the surface circulation is therefore not representative for the depth-averaged flow.

In contrast, the annual mean flow in the northern Indian Ocean is almost featureless, both in the Sverdrup circulation maps and in observations. The stream function map does not show a single streamline for the northern hemisphere, so any mean circulation that does develop must be weaker than 10 Sv (the contour interval used for Figure 4.7). This is, of course, a somewhat theoretical result since it represents the mean of two strong monsoonal current systems. The annual mean is still of use when it comes to the calculation of heat fluxes between the hemispheres, and we shall come back to this in Chapter 18. But in a discussion of monsoonal surface currents the Sverdrup relation has its limits, and we now turn to a description based on current and hydrographic observations.

During the Northeast Monsoon season the current system resembles closely those of the Pacific and Atlantic Oceans. The subtropical gyre dominates the southern hemisphere. For a long time it was believed that eastward flow in the south is achieved by the Circumpolar Current. Following the recent discovery of the South Atlantic Current as a distinct element of the south Atlantic subtropical gyre (Chapter 14), Stramma (1992) showed the existence of a similar South Indian Ocean Current north of the Circumpolar Current. The current follows the northern flank of the Subtropical Front, carrying some 60 Sv in the upper 1000 m southeast of Africa and gradually releasing its waters into the gyre. Southwest of Australia its transport is reduced to about 10 Sv. Zonal flow immediately south of the Subtropical Front is usually weak, indicating that the South Indian Ocean and the Circumpolar Currents are two distinct features of the circulation.

The subtropical gyre of the northern hemisphere is not well-defined; most of the water carried in the North Equatorial Current returns east with the Equatorial Countercurrent near 5°S, leaving little net transport for the weak currents in the northern Indian Ocean. The Equatorial Countercurrent continues into the South Java Current, which during this season feeds its waters into the Indonesian seas and southward into the South Equatorial Current. Currents flow in the opposite direction north of 10°S during the Southwest Monsoon season, when the South Equatorial Current intensifies and feeds part of its flow into the Somali Current, the western boundary current of the anticyclonic circulation that develops in the northern hemisphere. The North Equatorial Current disappears, and the Equatorial Countercurrent becomes absorbed into the Southwest Monsoon Current. Its broad eastward flow dominates the northern Indian Ocean.

A feature of the circulation which is independent of the monsoon cycle is the strong separation of the northern and southern hemisphere flow fields along the ITCZ east of 60°E. Little flow crosses the Doldrums east of the western boundary current. The semi-annual reversal of the intense flow across the ITCZ along the east African coast north of 10°N has been well documented during the last two decades. However, it is obvious that at least some of the water that enters the northern hemisphere from June to October in the west must leave it during that season. Likewise, at least some of the water that is withdrawn during December to April has to enter it somewhere in the east during these months. Our knowledge of the circulation near Java is, however, incomplete, and the details of the mass balance on seasonal time scales are a topic for the future.

The Indonesian throughflow from the Pacific Ocean enters the Indian Ocean during both seasons as a narrow band of low salinity water. It is embedded in generally westward flow and therefore apparently does not develop the strong lateral shear necessary to induce much instability. It continues westward, providing the core of maximum westward flow in the equatorial current system, and can be followed over the entire width of the Indian Ocean.

The subtropical gyre of the southern hemisphere is seen with two western boundary currents, one along eastern Madagascar and one along the coast of Mozambique. Whether both feed into the Agulhas Current - as indicated by the depth-integrated flow - or whether the East Madagascar Current feeds back into the gyre independently has been the subject of debate for some time and will be discussed in more detail later on. Here we only note the difference between the flow fields based on 1500 m and 2500 m levels of no motion (Figs 4.5 and 4.6) south of Madagascar; they indicate that the circulation near the end of the East Madagascar Current reaches deeper than 1500 m, not unlike the situation found in separation regions of other western boundary currents. The fact that deep flow is not restricted to the Agulhas Current but extends eastward away from Madagascar makes the estimation of transports in the gyre difficult and affects in particular our estimates for the South Equatorial Current.

The equatorial current system

Cutler and Swallow (1984) used the records of ship drifts collected by the British Meteorological Office from daily log book entries of merchant ships, to compile an atlas of surface currents. Currents in the Indian Ocean are stronger than in the Pacific or Atlantic Oceans during most of the year, which makes ship drift estimates reasonably reliable. Given the paucity of other information, this atlas is the best source of information on surface currents near the equator. Information on the subsurface structure became available with the long-term current meter moorings and time series of vertical current profiles taken during INDEX; unfortunately it is restricted to the region west of 62°E.

The evolution of surface currents through the seasons is shown in Figure 11.4. The *North Equatorial Current* is prominent in January and March when the Northeast Monsoon is fully established. It runs as a narrow current of about 0.3 m s^{-1} from Malacca Strait to southern Sri Lanka, where it bends southward and accelerates to reach 0.5 - 0.8 m s^{-1} between 2°S and 5°N in the region between 60°E and 75°E. The *South Equatorial Current* occupies the region south of 8°S with velocities rarely exceeding 0.3 m s^{-1}. Between these westward flows runs the *Equatorial Countercurrent* with 0.5 - 0.8 m s^{-1} in the west but getting weaker in the east; in January it does not reach beyond 70°E, being opposed in the east by weak westward flow.

The transition from Northeast to Southwest Monsoon (Figure 11.4c) is characterized by the intense *Indian Equatorial Jet* first described by Wyrtki (1973a). The long-term mean distributions derived from the ship drift data show it from early April until late June with velocities of 0.7 m s^{-1} or more. It is possible that in any particular year the jet appears within the three-month window April - June as a feature of shorter (one month) duration with higher peak velocities. The averaging employed with the ship drift data would spread it over the three months as a weaker feature. The jet is easily observed with drifting buoys since the current converges at the equator, keeping drifting objects trapped near its core. Away from the equator the current speed falls off to less than 0.2 m s^{-1} at 3°S or 3°N.

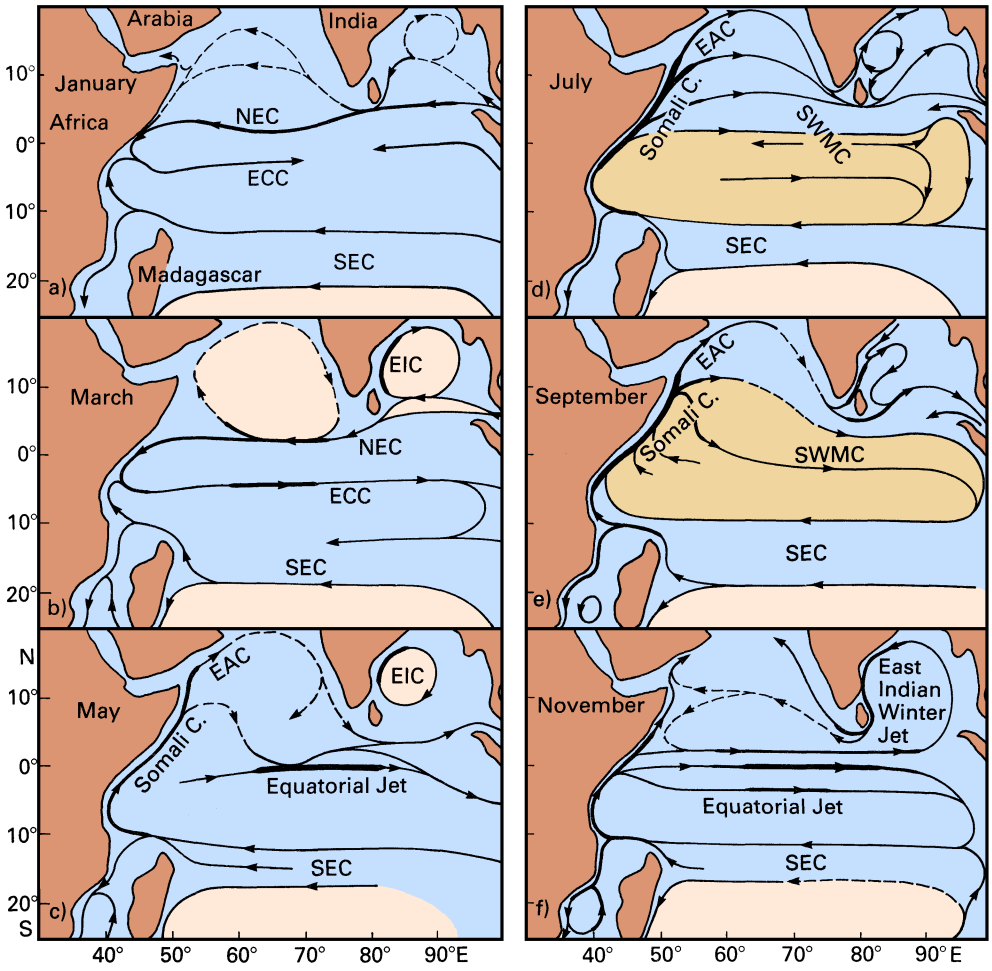

Fig. 11.4. Surface currents in the northern Indian Ocean as derived from ship drift data. SEC: South Equatorial Current, NEC: North Equatorial Current, ECC: Equatorial Countercurrent, SWMC: Southwest Monsoon Current, EAC: East Arabian Current, EIC: East Indian Current. Adapted from Cutler and Swallow (1984).

When the Southwest Monsoon is fully established during July and September, the entire region north of 5°S is dominated by the eastward flow of the *Southwest Monsoon Current*, the only exception being a narrow strip along the equator in July to which we shall return in a moment. Velocities in the Southwest Monsoon Current are generally close to 0.2 - 0.3 m s^{-1}, but an acceleration to 0.5 - 1.0 m s^{-1} occurs south and southeast of Sri Lanka. The South Equatorial Current expands slightly towards north, reaching 6°S in September. The transition before the onset of the Northeast Monsoon (Figure 11.4f) is again characterized by the Equatorial Jet. Concentrating all eastward flow in a 600 km wide

band along the equator it reaches its peak in November with velocities of 1.0 - 1.3 m s^{-1} and disappears in early January, when the annual cycle is repeated.

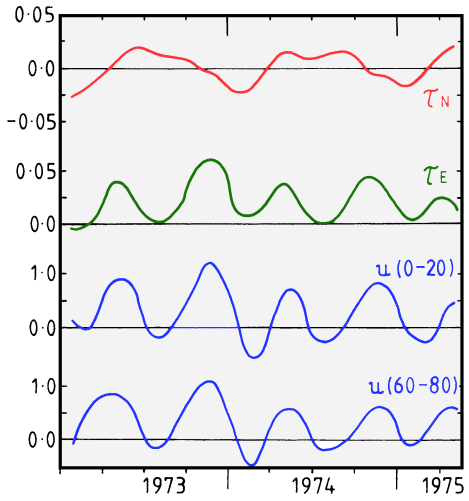

Fig. 11.5. Monthly mean winds and currents during 1973 - 1975 near the equator at 73°E: Meridional wind stress component τ_N (Pa), zonal wind stress component τ_E (Pa), and zonal velocities (m s^{-1}) averaged over 20 m for 0 - 20 m and 60 - 80 m depth. All directions indicate where currents and winds are going, north and east are positive. After McPhaden (1982).

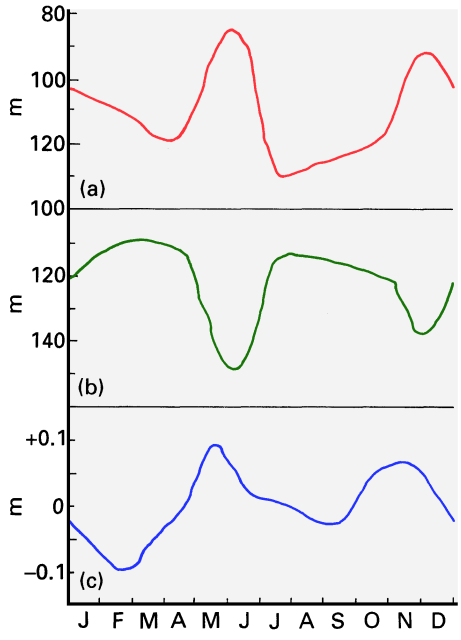

Fig. 11.6. Climatological mean monthly thermocline depth and sea level at the equator.

(a) Depth of 20°C isotherm off Africa,

(b) depth of 20°C isotherm off Sumatra,

(c) sea level at the west coast of Sumatra. After Wyrtki (1973a)

A remarkable feature of the equatorial current system is the dominance, within the annual monsoon cycle, of a semi-annual flow reversal in a narrow band along the equator. Figure 11.5 compares $2^1/_2$ years of wind data near the equator with average currents in two

layers above the thermocline. Winds at the equator are generally light, the meridional wind component being dominated by the annual monsoon cycle. The zonal wind component, on the other hand, shows westerly winds during the transition periods and exerts a strong semi-annual signal on the ocean. The associated change of current direction produces semi-annual variations in thermocline depth and sea level (Figure 11.6). The 20°C isotherm rises off Africa and falls off Sumatra during periods of eastward flow, indicating a net transport of 20 Sv in the equatorial band. The same transport in the opposite direction occurs during periods of westward flow when the 20°C isotherm rises off Sumatra and falls off Africa. The associated zonal slope of the thermocline finds its mirror image (as expressed in our Rule 1a of chapter 3) in the slope of the sea surface, as indicated by the sea level at Sumatra.

Figure 11.5 suggests a direct relationship between the zonal current and the zonal wind. However, the current is not purely wind-driven. An array of current meter moorings was deployed along the equator between 48°E and 62°E during INDEX (1979 - 1980), with instruments at 250 m, 500 m, and 750 m depth. The semi-annual current reversal occurred at all depths, much deeper than could be explained by direct wind forcing (Luyten and Roemmich, 1982). It appears that the wind reversal in the west is only the triggering mechanism for a wave phenomenon peculiar to the equatorial region known as a Kelvin wave. The same process is responsible for interannual climate variations in the equatorial Pacific Ocean which will be discussed in detail in Chapter 19. We therefore leave the explanation of Kelvin waves to that chapter and note here only the essence of the process, which is as follows. The arrival of westerly winds in the west lifts the thermocline up near the African coast. The resulting bulge in the thermocline travels eastward, accompanied by strong eastward flow, until it reaches Sumatra. Thus, eastward flow does not occur simultaneously but propagates along the equator. This explains why we find both eastward and westward flow at the equator on occasions, as in Figs. 11.4a and d.

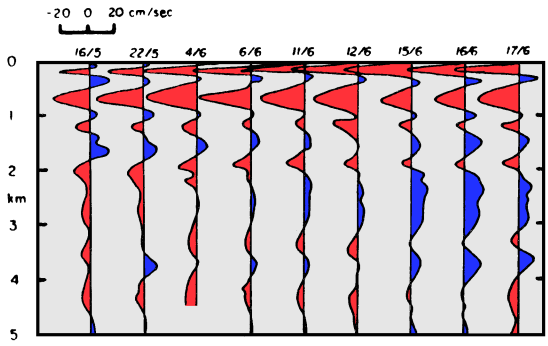

Fig. 11.7. Eastward components of velocity on the equator at 53°E. After Luyten and Swallow (1976).

The limited information available on subsurface flow near the equator indicates a complicated and unique current regime. Observations with profiling current meters show that the currents reach to great depth with only slightly reduced velocities (Figure 11.7). Several layers of alternate flow direction were found, with velocities reaching 0.12 m s^{-1} at 4000 m depth. The uppermost layer of westward flow near 200 m depth is commonly referred to as the *Equatorial Undercurrent*; but it is obvious that westward transport occurs at

much greater depths as well. During the Southwest Monsoon of 1976 mean flow at moorings in the area 52 - 58°E was westward with a northward component into the Somali basin at 500 m and 1500 m depth.

The oscillations of the undercurrent known from the Pacific and Atlantic Oceans occur in the Indian Ocean as well. At 200 m depth they were seen from August 1979 until January 1980 (in a record which covered the period March 1979 - June 1980). They were of 1300 km wavelength and 0.2 m s^{-1} meridional amplitude and shifted the undercurrent axis back and forth by about 150 km either side of the equator. Drifting buoy data for the period 1979 - 1982 indicate that at the peak of the Southwest Monsoon in August and September the oscillations reach into the surface layer with meridional flow amplitudes up to 0.8 m s^{-1}.

Circulation in the Arabian Sea and Bay of Bengal

Seasonal reversal of the currents dominates the two major subdivisions of the northern Indian Ocean as well, but the opposing flows occupy periods of very different length, and the transitions are less well defined than in the equatorial zone. Weak westward flow, an extension of the North Equatorial Current with velocities rarely exceeding 0.2 m s^{-1}, dominates in the Arabian Sea at the peak of the Northeast Monsoon season. Northwestward flow along the western Indian shelf begins as early as November (Figure 11.4f) and persists into January, with a width of some 400 km and a depth of about 200 m in the south (10°N), getting narrower and deeper as it flows along the continental slope. This current flows against the prevailing Northeast Monsoon and thus cannot be wind driven. The East Indian Winter Jet supplies fresh, low density water from the Bay of Bengal at this time, while on the north Indian coast cold continental winds result in cooling and convective overturn (Shetye *et al*., 1991). The resulting gradient of steric height overwhelms the wind forcing. These dynamics are discussed in more detail with the Leeuwin Current below.

Westward flow prevails south of 15°N and west of 65°E until late April, while in the remaining area currents are less and less well defined and change gradually into the weak anticyclonic pattern of Figure 11.4b. The Somali Current responds quickly to the onset of the Southwest Monsoon in April; northward flow develops, strengthening the pattern in the west. By mid-May (Figure 11.4c) the *East Arabian Current* is fully established with velocities of 0.5 - 0.8 m s^{-1}. At the same time the anti-cyclonic pattern breaks up from the east where the flow joins the Equatorial Jet around southern India and Sri Lanka. Moderate eastward flow, an extension of the Somali and Southwest Monsoon Current dominates the region during the next 4 - 5 months. During its peak in June and July it reaches 0.3 m s^{-1} and more but weakens rapidly in October when the second occurrence of the Equatorial Jet concentrates most eastward transport in the equatorial zone and outflow from the Bay of Bengal begins to oppose eastward flow around Sri Lanka. By mid-November currents are again diffuse; south of 15°N they are weak but already westward. General westward flow is again established by early December.

A notable feature of the Arabian Sea circulation is the occurrence of strong coastal upwelling in the East Arabian Current. As in other coastal upwelling regions it owes its existence to an offshore transport direction in the Ekman layer (the Southwest Monsoon blowing parallel to the coast with the coast on its left). Positive curl(τ/f) over a 400 km wide strip along the coast adds to the upwelling through Ekman suction. From May to

September coastal temperatures are lowered by 5°C and more (Figure 11.8). The fact that the upwelling is embedded in a western boundary current reduces its effectiveness for primary production - the swift current removes much of the additional biomass from the system before it can be utilized. Compared to upwelling regions in the Pacific and Atlantic Ocean, zooplankton levels in the Arabian Sea upwelling are much less exceptional. Nevertheless, an abundance of sea birds off the Arabian coast during the upwelling period indicates that it is sufficient to support a significant marine resource.

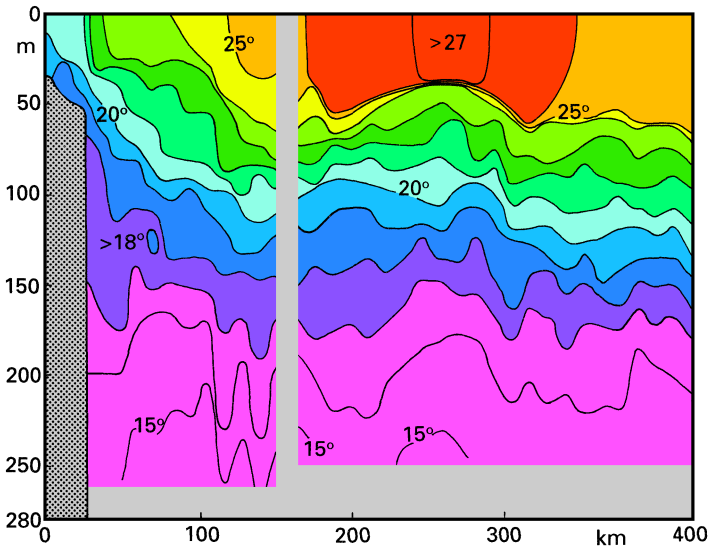

Fig. 11.8. A temperature section across the Arabian upwelling region during July 1983, from the Kuria Muria Islands (18°N) towards southeast. The break in the isotherm slope about 150 km from the coast separates the coastal upwelling to the left from the Ekman suction region to the right. After Currie *et al*. (1973).

An increase of zooplankton biomass associated with a drop in sea surface temperatures reminiscent of upwelling has also been documented for the western Indian shelf during the Southwest Monsoon season (Figure 11.9). Since the Southwest Monsoon cannot drive the surface waters offshore on that coast, the reasons for the increased productivity must be found elsewhere. Most likely the phenomenon is related to nearshore advection of river water associated with the monsoon rains and not to the oceanic circulation.

The circulation in the Bay of Bengal is characterized by anticyclonic flow during most months and strong cyclonic flow during November. In January currents are weak and variable. In the west, the *East Indian Current* strengthens as the Northeast Monsoon becomes stronger, exceeding 0.5 m s^{-1} in March (Figure 11.4b) and remaining strong (0.7 - 1.0 m s^{-1}) until May/June. Throughout this time the current runs into the wind, apparently as an extension of the North Equatorial Current. The fact that it persists during May when flow south of the Bay turns eastward is remarkable and still requires an explanation. During the Southwest Monsoon season currents in the entire Bay are weak and

variable again. The highest velocities (around 0.5 m s^{-1}) are found in the East Indian Current; flow along the eastern coast rarely exceeds 0.2 m s^{-1} but is often directed into the wind.

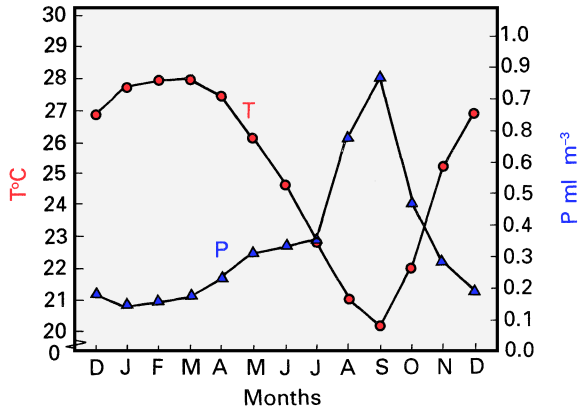

Fig. 11.9. Monthly mean temperature at 50 m depth (*T*) and zooplankton biomass (*P*) on the western Indian shelf between 8°N and 15°N. From Murty (1987).

An indication of a current reversal in the west is seen in September (Figure 11.4e). Currents are consistently southwestward and strong (0.5 m s^{-1} and more) north of 15°N, and close to the shelf southwestward flow prevails. Complete reversal of the East Indian Current into the *East Indian Winter Jet* is not achieved until late October, when water from the Equatorial Jet enters the Bay in the east and a cyclonic circulation is established. The East Indian Winter Jet is a powerful western boundary current with velocities consistently above 1.0 m s^{-1}. It follows the topography south of Sri Lanka and feeds its water into the Arabian Sea. Very little exchange occurs with the Equatorial Jet south of Sri Lanka; currents in the separation zone between the two jets (near 3°N) are weak and variable. The East Indian Winter Jet fades away from the north in late December, its southern part merging with the developing North Equatorial Current.

Western boundary currents

The story of the western boundary currents begins east of Madagascar, where both the integrated flow (Figure 4.7) and the ship drift currents show a separation of the South Equatorial Current into a northern and southern branch. The distribution of their transports - 30 Sv in the northern branch, 20 Sv in the southern branch - varies little over the year (Swallow *et al*., 1988). The contribution of the northern branch to the circulation in the southern hemisphere is the Mozambique Current; it is maintained throughout the year. The contribution to the circulation in the northern hemisphere ceases during the Northeast Monsoon season. The southern branch feeds the *East Madagascar Current*. The current field of this small but well-defined western boundary current reaches to the 2000 m level. Below 3100 m some 4 - 5 Sv are carried northward, with little movement in-between. Having passed the southern tip of Madagascar the current apparently alternates between three flow

patterns. A first path (*a* in Figure 11.10a) continues north along the west coast to return south with the Mozambique Current (*a*'). In the second path (*b*) the current flows directly west. Both paths feed into the Agulhas Current (*c*), going through a cyclonic loop (*d*) on their way. The third path, complete retroflection south of Madagascar (*c*'), cuts the East Madagascar Current off from the Agulhas Current; it is rarely followed by drifting buoys but occasionally seen in satellite data (Figure 11.10b).

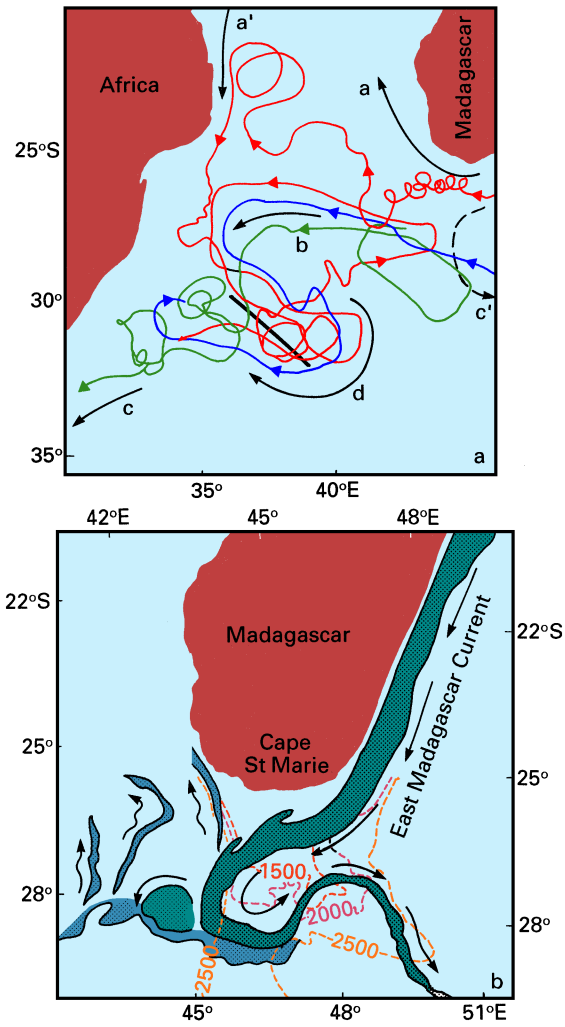

Fig. 11.10. Paths of the East Madagascar Current extension. (a) from tracks of satellite-tracked drifters, (b) from a satellite image of sea surface temperature on 13 June 1984. The warm core of the East Madagascar Current is indicated by dark shading. Light shading indicates intermediate water temperatures. The heavy line in (a) is the location of the section shown in Fig. 11.11. See the text for the meaning of letters in (a). After Lütjeharms *et al*. (1981), Gründlingh (1987) and Lütjeharms (1988).

The contribution of the *Mozambique Current* to the Agulhas Current is comparatively small. Although southward transport along the African shelf through Mozambique Strait was estimated at 30 Sv near 15°S, the Mozambique Current contributed only 6 Sv to this flow, the remaining 24 Sv coming from the northward looping East Madagascar Current (Zahn, 1984); in other words, the net southward transport near 15°S was only 6 Sv.

Entrainment of water from the loop increases the net southward flow to 15 Sv near 20°S. These estimates are based on a depth of no motion of 1000 m and do not include flow on the shelf, so they almost certainly underestimate the true transport of the Mozambique Current; but they leave little doubt that the East Madagascar Current is the more important source for the Agulhas Current.

The region south of Mozambique Strait is characterized by the frequent occurrence of cyclonic eddies (*d* in Figure 11.10), spawned by the passage of the joint flow from the Mozambique and East Madagascar Currents over the Mozambique Ridge. This ridge does not reach much higher than 1500 m; but the current reaches deep enough to be influenced by it. Figure 11.11 shows that the eddies are also deep-reaching energetic features, with life spans of many months and transports of 15 - 30 Sv.

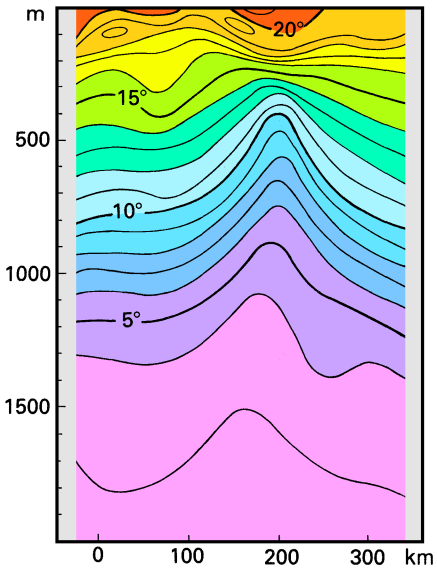

Fig. 11.11. A temperature section through a cyclonic eddy near the Mozambique Ridge. The form of the 3°C isotherm indicates that the eddy reaches deeper than 2000 m. See Fig. 11.10 for the location of the section. From Gründlingh (1985a).

South of 30°S the flow continues as the *Agulhas Current,* one of the strongest currents of the world ocean. In contrast to other western boundary currents it shows little seasonal variation. Mean speeds are 1.6 m s^{-1} throughout the year, and peak speeds exceed 2.5 m s^{-1} in most months. Transport estimates from observations give 70 Sv near 31°S and an increase of 6 Sv for every 100 km (as in the Gulf Stream). On approaching the shallow Agulhas Bank near 35°S it carries 95 - 135 Sv. The current occasionally floods the bank, lowering the inshore temperatures by several degrees (Figure 11.12). This upwelling is a result of the thermocline slope across the current (Rule 2 of Chapter 3) and not related to the wind. An increase in current speed increases the thermocline slope; since isotherm depths on the oceanic side of the current cannot change, the result is an uplift of cold water onto the shelf. Transport estimates for the Agulhas Current agree well with the depth-integrated estimate of Chapter 4 until the current rounds the Cape of Good Hope. Further south the current encounters the circumpolar eastward drift, and most of its transport turns back into the Indian Ocean (Figure 11.13), quite in contrast to the

prediction of Sverdrup theory which indicates a continuation of the current toward South America (Figs. 4.4 - 4.7). The reason for the striking departure from Sverdrup dynamics is that the current enters the Atlantic Ocean as a free jet and develops instabilities accompanied by eddy shedding, in a manner similar to the generation of East Australian Current eddies: The retroflection loop moves westward until its western part pinches of and the loop retreats to its most eastern position. (The two positions are indicated in Figure 11.13a by the crowding of front locations near 15°E and 19°E.) Most eddies are ejected into the Benguela Current and drift away toward northwest; in Figure 11.13c two eddies are seen by the depression of the thermocline in their centres (as explained with Figure 3.3). The eddies are among the most energetic in the world ocean and are believed to have life spans of many years. The associated transport of Indian Central Water into the Atlantic Ocean is an important element in the recirculation of North Atlantic Deep Water (see Chapter 7). Observations show that net transfer of water between the two oceans is westward in the thermocline (above 1500 m) but eastward underneath. Estimates for the time-averaged transfer of thermocline water from Agulhas Current eddies range from 5 to 15 Sv.

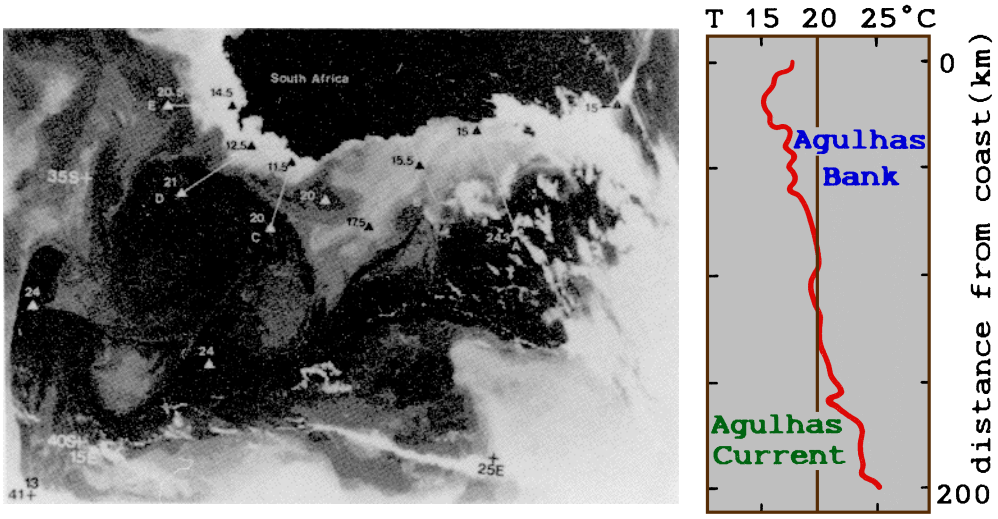

Fig. 11.12. Upwelling over the Agulhas Bank induced by the Agulhas Current. (a) Satellite image of sea surface temperature (dark is warm; small light patches are clouds. Numbers next to triangles are temperature in °C), (b) Temperature section along the track labelled *A* in (a). From Walker (1986).

Near 25°E the Agulhas Plateau which reaches above 2500 m depth causes a northward excursion and further instability in the path of the retroflection current. The feature is seen in the frontal positions of Figure 11.13a; it was observed as early as 1899 when the steamer *Waikato* broke down on the Agulhas Bank and drifted in the current for 100 days; it rounded the Agulhas Plateau, looped through two eddies, and drifted eastward, reaching 65°E after a journey of 5000 km.

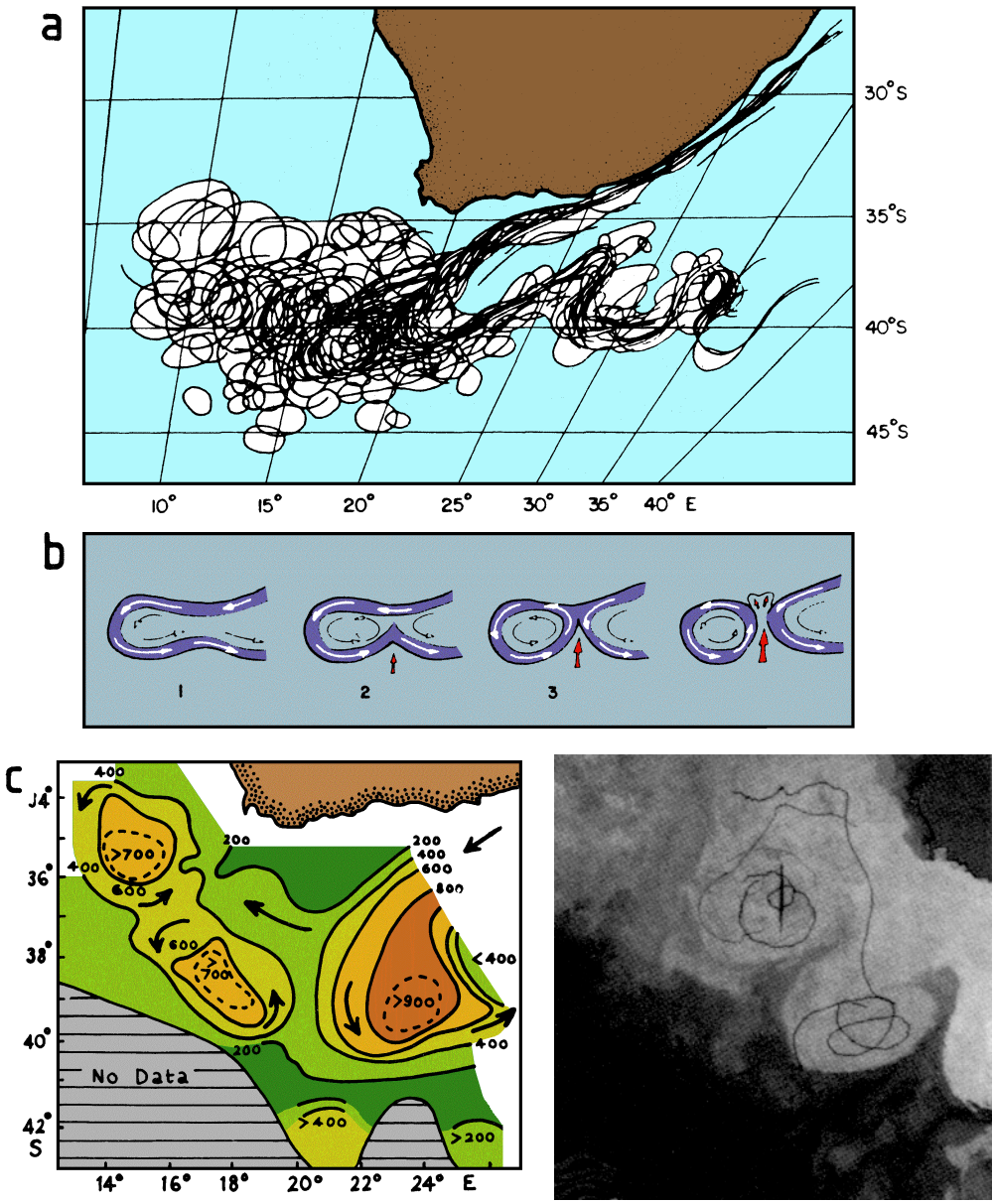

Fig. 11.13. The retroflection region of the Agulhas Current. (a) Positions of the temperature front along the Agulhas Current for a 12 month period 1984/85; (b) sketch of the eddy shedding process at the retroflection; (c) depth of the 10°C isotherm (representative for the thermocline) in November/December 1983; (d) sea surface temperature during 7 - 9 December 1983 and tracks of drifting buoys in November/December 1983. The area shown is approximately 32° - 42°S, 10° - 20°E. To minimize cloud disturbance the picture is a composite of three images. Lighter tones indicate warmer water. From Lütjeharms and van Ballegooyen (1988) and Gordon (1985).

Winds near southern Africa are westerly to southwesterly throughout the year, bringing cold unsaturated maritime air over the Agulhas Current system. Unlike the Gulf Stream and Kuroshio the Agulhas Current therefore loses heat during all seasons. On average annual net heat loss amounts to 75 W m^{-2}, less than half of the values found in the northern hemisphere. A unique aspect of the region is that the Mozambique, East Madagascar, and Agulhas Currents all run against the prevailing wind direction during the Southwest Monsoon season. This produces a steepening of the wind waves. Further south the current runs into the mature swell of the Southern Ocean. The resulting steepening of the swell produces some of the most dangerous waves of the world ocean; with wave heights of 20 m and more and a steepness that can cause ordinary wind waves of the open ocean to turn into breakers they are capable of inflicting severe damage on the largest vessels.

North of 10°S the East African Coastal or *Zanzibar Current* flows northward, fed by the northern branch of the South Equatorial Current. Because of its permanent character it is well resolved in the vertically integrated flow (Figure 4.7). During the Northeast Monsoon season it runs against light winds and is opposed by the southward flowing Somali Current. The point where northward and southward flows meet at the surface moves from 1°N at the beginning of the season to 4°S during the February peak, when the Zanzibar Current is at its weakest. Soon after the peak it starts moving north again, reaching the equator by early April. Throughout this period the current feeds into the Equatorial Countercurrent. Below the surface flow the Zanzibar Current flows northward across the equator at all times, taking the form of an undercurrent under the southward flowing Somali Current during the Northwest Monsoon season (Figure 11.14). During the Southwest Monsoon season the strength of the Zanzibar Current increases considerably; INDEX observations from April/May 1979 show it with speeds of 2.0 m s^{-1} and a transport of 15 Sv. The current now feeds the northward flowing Somali Current; some consider it part of the Somali Current during these months.

Southward flow in the *Somali Current* during the Northeast Monsoon is limited to the region south of 10°N. It first occurs in early December south of 5°N and expands rapidly to 10°N in January (Figure 11.4a) with velocities of 0.7 - 1.0 m s^{-1}. In March the southward flow contracts again to 4°N, until the surface flow reverses in April. During the Southwest Monsoon the Somali Current develops into an intense jet with extreme velocities; INDEX observations gave surface speeds of 2.0 m s^{-1} for mid-May and 3.5 m s^{-1} and more for June.

South of 5°N the Somali Current is extremely shallow; below 150 m depth southward flow is maintained throughout the year (Figure 11.15). Further north the jet deepens, eventually embracing the permanent thermocline. The current structure on the equator is extremely complex and shows layering similar to the equatorial flow further east (Figure 11.7) but oriented northward-southward.

The period of northward flow can be divided into two phases of different dynamics. During the transition in May, flow in the Equatorial Jet is eastward, and westward flow develops only slowly during the following two months. From the point of view of mass continuity there is not much need for a strong western boundary current until the monsoon reaches its peak in August, and the Somali Current is first established as a response to the wind reversal along the African coast. Winds are southerly but light in late April and May and strengthen abruptly in late May or June. This drives northward flow across the equator; but the flow turns offshore near 3°N, and a coastal upwelling regime develops between 3°N and 10°N. Figure 11.16a displays this division into two separate northward flows in the sea

surface temperature for May/June 1979. The dynamic structure of the upwelling region is identical to that of other coastal upwelling regimes (see for example the Peru/Chile upwelling in Chapter 8); the southward flow beneath 150 m mentioned above is in fact the continuation of its undercurrent. The increase in wind speed four weeks later strengthens the oceanic circulation, without destroying the two-gyre structure (Figure 11.17); current speeds can reach 3.5 m s^{-1} at the surface, and coastal temperatures in the two upwelling centres are lowered dramatically (Figure 11.16b). Reported transport estimates are 27 Sv above 100 m and 80 Sv between the surface and 700 m for the southern gyre, and 22 Sv above 100 m in the northern gyre. As the monsoon reaches its peak in August, the temperature front at 4°N is pushed northward along the coast until it merges with the Ras Hafun front; by September the Somali Current is established as a continuous western boundary current, from the Zanzibar Current in the south to the East Arabian Current in the north. The Ras Hafun gyre survives offshore as the "Great Whirl", keeping mixed layer depths greater than 200 m near 9 - 10°N, 53 - 54°E during the November transition and early Southwest Monsoon season when mixed layer depths are near 50 m elsewhere.

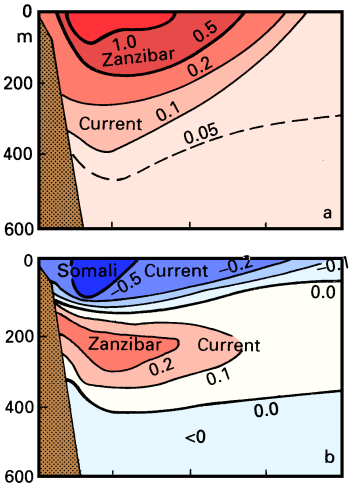

Fig. 11.14. (Left) Mean meridional current velocity (m s^{-1}) in the western boundary currents at the equator, derived from 2 years of observations during 1984 - 1986. (a) June - September, (b) December - February. After Schott *et al*. (1990).

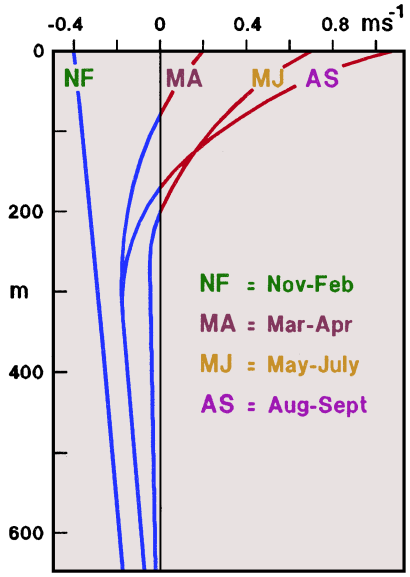

Fig. 11.15. (Right) Mean alongshore velocity (positive = northeastward) in the Somali Current at 5°N, from 30 months of current meter records. After Quadfasel and Schott (1983).

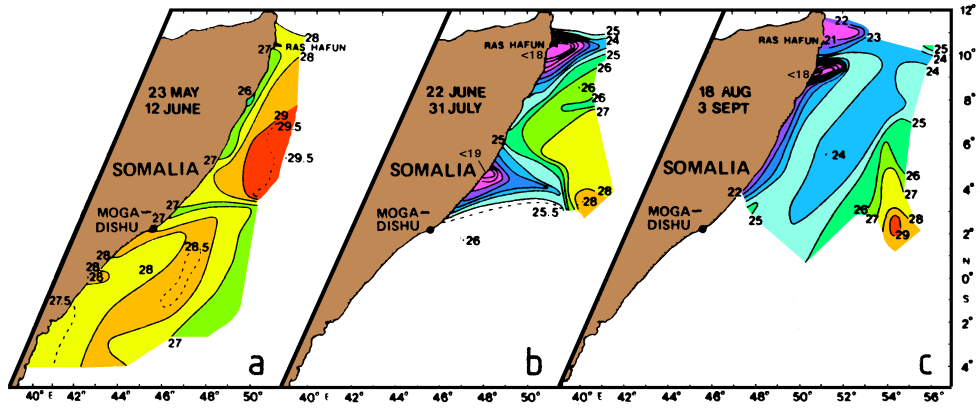

Fig. 11.16. Development of the Somali Current during the onset of the Southwest Monsoon as seen in the sea surface temperature during 1979. (a) Advection of warm water south of 3°N and coastal upwelling north of 3°N, (b) two gyres with upwelling regions near 4°N (minimum temperature <19°C) and Ras Hafun (minimum temperature <18°C), (c) continuous northward flow and upwelling near Ras Hafun (minimum temperature <17°C). From Evans and Brown (1981).

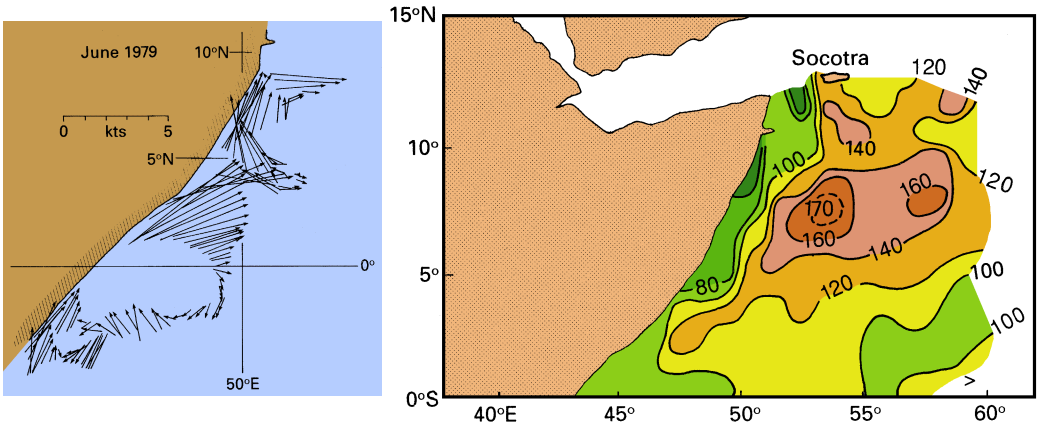

Fig. 11.17. The two-gyre phase of the Somali Current. (a) Surface currents in June 1979 along the track of *Discovery*, (b) the northern gyre as seen in the mean depth of 20°C isotherm (m) during June. This eddy is often called the "Great Whirl". From Swallow and Fieux (1982) and Bruce *et al*. (1980).

Eastern boundary currents

The eastern boundary of the tropical Indian Ocean is different from the Atlantic and Pacific eastern boundaries in several respects. First, the mean temperature and salinity stratification is less developed than off Peru and West Africa, so when upwelling occurs it

generally does not generate marked surface cooling. Secondly, the monsoon wind reversal is so complete along this coast that the annual mean alongshore wind stresses here are close to zero, from the northern Bay of Bengal south to Java (Figure 1.4) and the upwelling in one season is counteracted by downwelling in the following season. Thirdly, twice a year (around May and November) the Equatorial Jet feeds warm water towards Sumatra, generating a pulse of current that flows poleward in both hemispheres. The seasonal cycle thus has strong semiannual as well as annual components, and is quite complicated. The strongest westward currents along the southern coast of Java, the seasonally reversing *South Java Current*, occur in August, when the monsoon winds are easterly and the Equatorial Jet is inactive. Surface cooling occurs off South Java at this time. This is also the time when the sea level difference from Java to Australia is largest, implying maximum strength in the Indonesian throughflow (see Chapter 13) and suggesting that at least some of the water for the South Java Current is then supplied from the Pacific Ocean.

The dynamics of the eastern boundary current along the western Australian coast, known as the *Leeuwin Current*, are very unusual and require some explanation. In the Pacific and Atlantic Oceans equatorward winds along the eastern boundary produce coastal upwelling, an equatorward surface flow, and a poleward undercurrent. In the Indian Ocean, annual mean winds along western Australia do blow towards the equator, but at the surface a vigorous poleward flow runs against the wind, and the undercurrent is equatorward. The reason is that eastern boundary currents are driven by the combined effects of alongshore winds and alongshore pressure gradients in the upper ocean. Figure 2.8b demonstrates that the upper ocean pressure distribution in the Indian Ocean differs substantially from those of the other oceans. While variations in dynamic height in the subtropics do not exceed 0.1 $m^2\ s^{-2}$ along most eastern coastlines, this difference is 0.5 $m^2\ s^{-2}$ (equivalent to about 0.5 m steric height) along western Australia. In the open ocean it drives an eastward geostrophic flow; but closer to the coast eastward flow becomes impossible, and the water accelerates down the pressure gradient. In the Indian Ocean the resulting poleward flow is strong enough to override the wind-driven equatorward current — and the onshore geostrophic flow is strong enough to override the offshore Ekman flow.

The large drop in steric height along western Australia is apparently related to the connection between the Pacific and Indian Oceans through the Australasian Mediterranean Sea. The free connection from the Pacific to the Indian Ocean permits steric height to have similar values at either end of the channel — i.e. the steric height off Northwest Australia is essentially the same as in the western equatorial Pacific Ocean (Figure 2.8b). Steric height is about 0.5 m larger than that off Peru, because the easterly winds blowing along the equatorial Pacific Ocean maintain the steric height gradient along the equator that can be seen in Figure 2.8b. The high steric height at 15°S off northwest Australia cannot be maintained at 34°S — steric height is primarily a depth-integral of temperature through eqn (2.3), and to maintain the same surface steric height at 34°S would require maintenance of an average temperature of about 25°C over the top 200m, in a region where strong winds and air temperatures of 12°C occur in winter. Strong cooling and convective overturn occurs (Figure 11.18), to bring water temperatures down nearer to air temperatures throughout a mixed layer typically 150m deep, near 34°S in winter. This heat loss can be seen in Figure 1.6, which shows that, unlike the other eastern boundaries, a net heat loss to the atmosphere occurs near the western Australian coast poleward of 20°S. It extends down to 150 m and results in relatively low steric height at the southern end of western Australia. The resulting southward flow in turn feeds the warm water pollards to maintain the surface

heat loss. The process is self-perpetuating, as southward flow is accompanied by surface cooling, and surface cooling produces southward flow.

As mentioned before, the dynamics of the currents along the western Indian shelf during the Northeast Monsoon are similar to those of the Leeuwin Current. In the northern hemisphere case the large alongshore steric height gradient is the result of differences in water temperature and salinity produced by the monsoon winds combined with seasonal cooling.

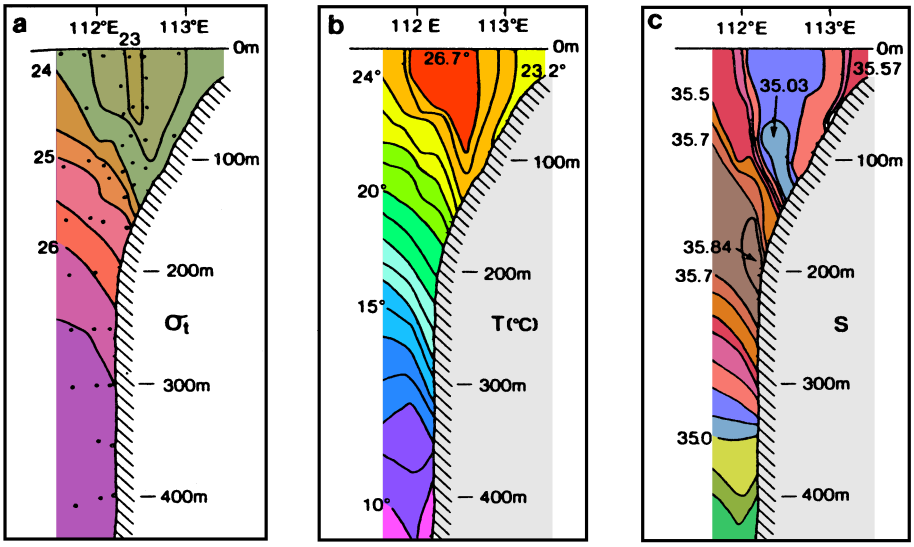

Fig. 11.18. Hydrographic properties in the Leeuwin Current near 25°S. (a) Density, (b) temperature (°C), (c) salinity. Note the deep mixed layer produced by convective cooling between 112°E and 113°E. From Thompson (1984).

The annual mean transport of the Leeuwin Current is estimated at 5 Sv, with average current velocities of 0.1 - 0.2 m s^{-1}. However, the intensity and southward extent of the current vary strongly with the seasons, in response to variations in the southerly wind and perhaps also the alongshore pressure gradient. The southerly wind is weakest in May. At this time the Leeuwin Current passes round Cape Leeuwin at speeds of up to 1.5 m s^{-1} and enters the Great Australian Bight. The associated advection of warm low salinity water produces a distinct seasonal cycle in the water properties along the western Australian coast (Figure 11.19) and hydrographic fronts on the offshore and inshore edges of the current (Figure 11.20). Eddies produced by the strong current shear across the fronts are clearly visible in satellite images of sea surface temperature (Figure 11.21).

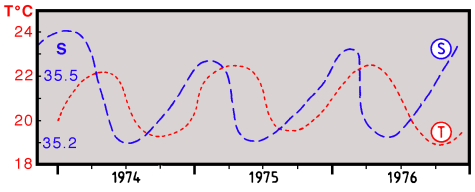

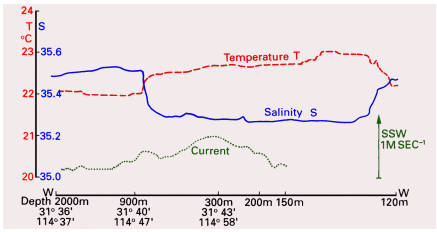

Fig. 11.19. (Left) Seasonal variation of surface temperature (*T*) and salinity (*S*) on the central shelf off Perth (32°S). Note the rapid drop of salinity between March and June; the Leeuwin Current is at its peak around April/May, bringing warm, fresh water from the tropics. From Cresswell and Golding (1980).

Fig. 11.20. (Right) A section across the Leeuwin Current off Perth (31°40'S), showing temperature and salinity fronts near 900 m and 120 m water depth on either side of the current. From Cresswell and Golding (1980).

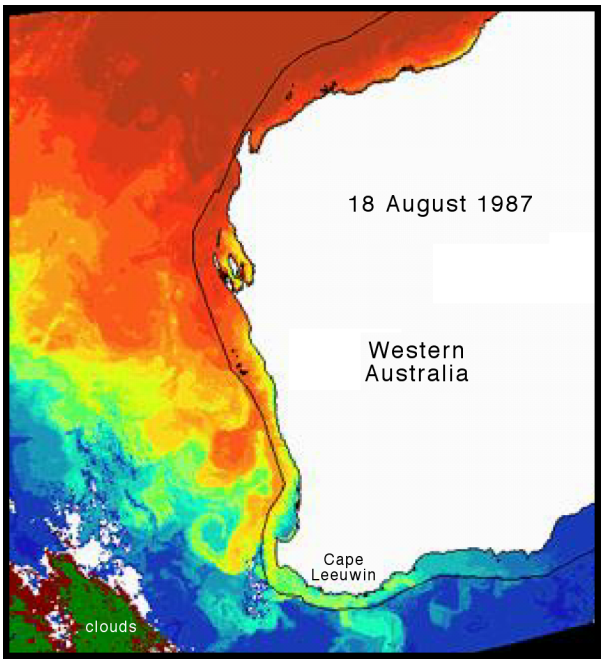

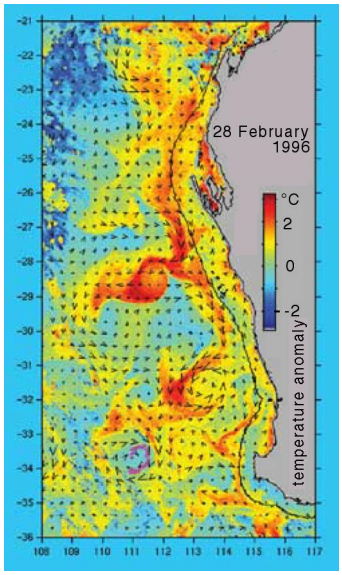

Fig. 11.21. Satellite images of sea surface temperature in the Leeuwin Current and associated eddies. Warm is red, cold is blue. Left: Sea surface temperature in August 1987. The Leeuwin Current is seen as a band of warm water along the western coastline that continues around Cape Leeuwin. The black line indicates the shelf break. (b) Sea surface temperature anomalies (departures from the latitudinal mean temperature) in February 1996 showing large eddies near Cape Leeuwin. Black arrows indicate surface currents. © CSIRO Marine Research, reproduced by permission.